journal of the mechanical behavior of biomedical materials 156 (2024) 106607

Contents lists available at ScienceDirect

Journal of the Mechanical Behavior of Biomedical Materials

journal homepage: www.elsevier.com/locate/jmbbm

Influence of surface finishing on the outcome of a 3-point bending test in polymer-based dental composits assessed by qualitative and quantitative fractography

Nicoleta Ilie

Department of Conservative Dentistry, University Hospital, Ludwig-Maximilians-University, Goethestr. 70, D-80336, Munich, Germany

ARTICLE INFO

Keywords:
Composites
Fractography
3-Point-bending test
Strength
Fracture mirror

ABSTRACT

Objectives: The aim of the study was to evaluate the influence of surface finishing in three polymer-based composits (composits) on the result of a 3-point bending test using quantitative and qualitative fractography as well as microstructural characteristics.

Materials and methods: 270 rectangular specimens (n = 30) of three composits were prepared, stored and tested according to NIST No. 4877. Prior testing, the samples were subjected to three surface treatments: 1) no treatment, to preserve the oxygen inhibition layer, 2) with FEPA P1200 (ANSI equivalent grit 600) SiC paper abraded surface, and 3) polished surface. A three-point bending testing was employed, followed by quantitative (assessment of reason for failure and fracture pattern) and qualitative (fracture mirror measurements) fractography, 3D and 2D surface imaging, surface roughness, reliability and Fe-SEM analysis. The mirror radius that runs in the direction of constant stress was used to calculate the mirror constant (A) using Orr's equation. Uni- and multifactorial ANOVA, Tukey's post hoc test, and Weibull analysis was performed for statistical analysis.

Results: Surface finishing has less influence on the fracture pattern, reliability and mechanical parameters and has no influence on the mirror constant. The amount of inorganic filler has a direct impact on flexural strength and modulus, while the ranking of materials was independent of surface treatment. Failures initiated by volume defects were the most common failure mode (77.0%) with surface defects accounting for 14.9% (edge) and 7.7% (corner). Polishing resulted in lower peak-to valley height compared to no treatment, both 3–4 times lower compared to the 600 grit treatment. The increase in roughness within the analyzed range did not lead to an increase in surface-related failures.

Conclusions: The clear dominance of volume defects in all examined materials as a cause of material fracture reduces the impact of roughness on the measured properties. This insight was only possible using qualitative and quantitative research fractography.

1. Introduction

Light-curing polymer-based composites (composites) have undergone major changes over the decades in terms of their microstructure, filler loading, type and distribution (Ferracane, 2011), with a clear trend towards miniaturization of filler size to adapt to the increasingly higher aesthetic demands. The latter is indispensably linked to the polishability and polish retention of the materials (Amaya-et al., 2022). Aside from aesthetic considerations, rough surfaces caused by improper finishing of restorations and large filler sizes are clinically associated to increased plaque accumulation, gingival irritation, or staining (Bollen et al., 1997).

The mixing process of the individual material components during the preparation of the composite paste as well as the processing (layering) and shaping during clinical or in-vitro material application may introduce flaws in the final filling or composite sample. These can be either voids, large fillers poorly integrated into the organic matrix, microstructural heterogeneities, filler agglomerates or inclusions that can be located both on the surface and in bulk. Surface processing of the hardened composite material, including grinding and polishing, can also create flaws by roughening the surface or exposing volume flaws. Another particularity of composites is the fact that an oxygen inhibition layer is created on the surface of unprocessed samples, which has different properties compared to the deeper layers of the material

E-mail address: nicoleta.ilie@med.uni-muenchen.de.

https://doi.org/10.1016/j.jmbbm.2024.106607
Received 12 April 2024; Received in revised form 24 May 2024; Accepted 29 May 2024
Available online 31 May 2024

(Gauthier et al., 2005).

Although the polymer matrix, as an essential part of the composition, has a plastic character, the high inorganic filler content, which necessarily serves to improve the mechanical properties enabling clinical application also in large fillings in areas exposed to high mechanical stress, provides composite materials a brittle character (Ferracane, 2011). These facts have led to the principles of brittle fracture mechanics increasingly being tested and applied (Quinn et al., 2007) to characterize composite materials. As a pioneer in the application of the quantitative and qualitative fractography in dental materials Quinn et al. (2007) proved that what was used in brittle dental ceramics can be in large parts transferred for the analysis of indirect composites in-vitro (Quinn and Quinn, 2010). Following in-vitro analysis, fractographic techniques have been developed to characterize also in-vivo failed glass, ceramic (Quinn et al., 2005; Lohbauer et al., 2010) and fiberglass-reinforced composite restorations (Scherrer et al., 2006, 2017) and have been expanded over the years to increasingly advanced clinical areas such as implant restorations (Øilo and Arola, 2018) or fixation screws in implant-supported restorations (Aboushelib and Elraggal, 2023), which makes them established and recognized examination methods today.

Fracture in composites is initiated from a critical flaw potentially originated from any of the sources enumerated above that is liable to propagate as crack (Quinn et al., 2007). In this connection, Griffith defined for brittle materials an inverse relationship between the square root of the flaw length and the stress at fracture (Griffith and Taylor, 1921). As the fracture propagates, a smooth radial region, the fracture mirror, forms (Johnson and Holloway, 1966) in moderate to high-strength samples. The shape of the fracture mirror is generally circular or semicircular, but may be altered due to stress gradients or geometrical effects (Quinn, 2007). In this context, the size and shape of the critical flaws (Mecholsky et al., 1974) as well as additional flaws encountered during crack propagation can either elongate the primary mirror or induce the formation of secondary mirrors (Bansal and Duckworth, 1977). The fracture mirror is delimited by an area termed mist, formed by secondary cracks that can no longer propagate due to decreasing energy (Yoffe, 1951), and which form when the crack tip deviates from the main plane. An area of larger radial ridges followed, the hackle lines, which led to macroscopic crack branching (Kirchner and Conway, 1987). The formed mirror and its dimension are valuable fractographic information, as the fracture stress and mirror radius measured along the tensile surface (Mecholsky et al., 1976) was shown to follow a −0.5 power law. This relationship is defined by the Orr equation and allow the calculation of the mirror constant (A), a material parameter that has been shown to correlate with the critical fracture toughness K_{Ic} (Mecholsky et al., 1976), while the relationship depends on the mirror-to-flaw size ratios. The applicability of the Orr equation to composite materials has already been confirmed (Quinn et al., 2007; Ghelbere and Ilie, 2023).

Differences in microstructure, particularly filler size, type and distribution, suggest that in addition to inherent flaws, different surface treatments may individually impact the properties of composite materials. It is also often observed that additional processing of the sample surface is not carried out in in-vitro tests because this is considered complex and cost-intensive. A conceivable impact on frequently used methods for determining the strength of composite materials, including the three-point bending test, can therefore be assumed. The literature search reveals little systematic research on this topic. For glass ceramics, an older study showed that the roughness limit at which strength begins to decrease was 0.65 μm, achieved by roughening with a 1000-grit silicon carbide abrasive paper, while for an older light-curing composite it was 2.1 μm (grit 320) (Lohbauer et al., 2008). Since the standardized test (ISO 4049 (ISO 4049)) is used to select materials that can be placed in load-bearing areas of posterior restorations, the influence of surface treatment requires thorough investigation. The aim of the present study was therefore to define the influence of surface finishing of modern composite materials with different chemical compositions and filler amounts on the result of a three-point bending test. Qualitative fractography should identify critical flaw locations and fracture patterns, quantitative fractography should enable calculation of the mirror constant and be related to microstructural analysis and 3D topography data.

The null hypotheses tested state that surface treatment, which was either no treatment to preserve the oxygen inhibition layer, with 600-grit (P1200) SiC paper abraded surface or polished surface, has no effect on the a) 3-point bending test results (flexural strength and modulus, beam deflection); b) qualitative (fracture pattern, location of critical flaw), and c) quantitative fractographic parameters (mirror constant).

2. Materials and methods

2.1. Materials

Three hybrid dental polymer-based composites with different viscosity, chemical composition and microstructure were employed (Table 1), while the sample surface was subjected to three different treatments. For this purpose, an Ormocer-based composite (organically modified ceramic) with silica fillers (Admira Fusion 5, AF5), a universal hybrid composite with a wide variation in filler size and distribution (Venus, V), and a flowable composite with bioactive surface pre-reacted glass fillers (Beautifil Flow Plus F03, BFP) were selected.

Composites were cured with a violet-blue LED (Light Emitted Diode) LCU (Light Curing Unit) (Bluephase® Style, Ivoclar Vivadent, Schaan, Lichtenstein, irradiance (1405 ± 12) mW/cm^2 (n = 5), measured with a spectrophotometer (MARC, Managing Accurate Resin Curing) system; Bluelight Analytics Inc., Halifax, Canada) according to the manufacturer recommendation, which was 10 s for AF5 and BFP and 20 s for V.

2.2. Methods

The mechanical parameters of the composites were determined at macroscopic level in a three-point bending test after receiving three different surface treatments and complemented by qualitative and quantitative fractography, reliability and roughness analysis, as well as light and Fe-SEM microscopy.

2.2.1. Three-point bending test

A total of 270 rectangular parallelepiped specimens (2 mm × 2 mm × 18 mm, n = 30) of three RBCs were prepared in a white polyoxymethylene mold according to the recommendation of ISO 4049:2019 (ISO 4049) for the 3-point bending test. Light exposure followed the

Table 1
Analyzed RBCs: Abbreviation (code), brand, manufacturer, shade, LOT and composition, as indicated by the manufacturer.

Code	Material/Shade	LOT	Monomer	Filler	
				Composition/size	wt/vol%
AF5	Admira Fusion 5 VOCO (A2)	V97552	Ormocer	SiO_2	84/-
V	Venus Kulzer (universal shade)	K010518	Bis-GMA TEGDMA	Ba–Al–B–F–Si glass, SiO_2	78/59
BFP	Beautifil Flow Plus F03 Shofu Inc. (A2)	011876	Bis-GMA TEGDMA	S-PRG Al–B–F–Si glass, PPF	67/-

Abbreviations: Bis-GMA = bisphenol A glycol dimethacrylate; TEGDMA = Triethylene glycol dimethacrylate; SiO_2 = silicon oxide (silica); Ba–Al–B–F–Si glass = $BaO–Al_2O_3– B_2O_3–F–SiO_2$ (Barium Aluminium Boro Fluor Silicate) glass; S-PRG = surface pre-reacted glasses; PPF = pre-polymerized fillers; wt % = percent by weight; vol % = percent by volume; "-" = not stated.

protocol specified in the standard, which included irradiation on the top and bottom of the samples for 10 s (AF5 and BFP) or 20 s (V), with three light exposures overlapping an irradiated section by no more than 1 mm of the light guide diameter to prevent multiple polymerizations. Immediately after light exposure, specimens were removed from the mold and immersed in distilled water at 37 °C for 24 h. One third (n = 90) of the test specimens (n = 30 per material) were wet-ground with silicon carbide paper (FEPA P1200, which corresponds to ANSI grit 600, Leco Corp. SS-200, MI, USA), while considering all four large (18x2) mm^2 surfaces of the parallelepiped specimen. One third of the specimens, involving again all four (18x2) mm^2 surfaces, were wet-ground with a continuously finer silicon carbide abrasive paper (grit p1200, p2500 and p4000, LECO Corporation, Saint Joseph, MI, USA) and polished with a diamond suspension (mean grain size: 1 μm) for 2–3 min, until the surface was shiny (automatic grinding machine, EXAKT 400CS Micro Grinding System EXAKT Technologies Inc., Oklahoma City, OK, USA). To ensure that the entire surface was ground, marks were placed randomly on the surface of the samples; By grinding off all markings, plane parallelism was accepted. During grinding, the device head, which holds the samples firmly due to vacuum generation, was loaded with 182 g. The final third was left untreated to preserve the oxygen inhibition layer that forms on all composite sample surfaces during polymerization. If any thin excess material after pressing the material in the mold was observed, it was retained.

The flexural strength (FS), flexural modulus (E) and beam deflection (ε) were determined in a 3-point bending test according to NIST No. 4877 and considering a span of 12 mm (Quinn, 1992). Therefore, samples were loaded in a universal testing machine until fracture (Z 2.5 Zwick/Roell, Ulm, Germany) at a crosshead speed of 0.5 mm/min. The force in bending was measured as a function of beam deflection, and the slope of the linear part of this curve was used to calculate the flexural modulus.

2.2.1.1. 3D surface imaging and 2D roughness analysis. Three test specimens per material and surface treatment were randomly selected from the fragments of the 3-point bending test. 3D imaging was performed on 300 μm × 200 μm areas by means of a 3D laser scanning microscope (VK-X3000, Keyence, Osaka, Japan; 408 nm violet laser light; lateral resolution of the microscope 120 nm). The microscope scanned the surface using a 16-bit photomultiplier to receive the reflected laser light. The 2D parameters Ra (arithmetic average of profile height deviations from the mean line) and Rz (peak to valley height) were calculated as the average of nine line profiles, three on each zone. The direction of the selected profiles was perpendicular to the sliding direction.

2.2.1.2. Fracture surface topography and fractography analysis (light microscopy). The qualitative and quantitative fractography was performed with a stereomicroscope (Stemi 508×, Carl Zeiss AG, Oberkochen, Germany, 40× magnification) on all fractured specimens. Both halves of the 270 broken test specimens were examined, i.e. 540 surfaces in total, with the half with the most clear traces of brittle fracture being further photographed and evaluated using a microscope extension camera (Axiocam 305 color, Carl Zeiss AG, Oberkochen, Germany). Qualitative fractography involved locating the fracture origin and determining the fracture pattern. The origin of fracture was identified either as volume (sub-surface) or surface (edge, corner) defects.

Quantitative fractography then evaluated the characteristics and properties of the fractured surface in terms of fracture mirror and fracture mirror radius. Therefore the mirror boundaries corresponded to the first signs of perceptible roughness after the relatively smooth mirror region were identified. The mirror radius (R), which runs in the direction of constant stress, i.e. parallel to the tensile side of the sample, from the origin of the fracture to the mirror boundary (ImageJ Version 1.53k, U.S. National Institutes of Health, Bethesda, MD, USA) was then measured. If the origin of the fracture could not be accurately identified, the diameter of the mirror was measured and then halved to identify the corresponding radius.

The measured strength (σ) and mirror radius (R) were further used to determine the mirror constant (A), based on the Orr equation (Orr, 1972):

$$\sigma\sqrt{R} = A \quad \text{(Equation 1)}$$

2.2.1.3. Field-emission scanning electron microscopy. The structural appearance of the filler system was examined for each material by field-emission scanning electron microscopy (Fe-SEM) using an electron backscatter diffraction approach (Zeiss Supra 55VP, Carl Zeiss GmbH, Göttingen, Germany) and up to 3000× magnification. Therefore, specimens were wet-ground, as described above, with a continuously finer silicon carbide abrasive paper (grit p1200, p2500 and p4000), and polished with a diamond suspension (mean grain size: 1 μm).

Three samples per material and surface treatment were examined in order to characterize the surface condition after the respective treatment. In addition, representative recordings for each fracture pattern observed in the light microscopic evaluation were also documented using scanning electron microscopy.

2.3. Statistical analyses

The distribution of the variables was tested using the Shapiro-Wilk method. Since the variables were normally distributed, a parametric approach followed. The homogeneity of variance was initially confirmed. One- and multiple-way analysis of variance (ANOVA) and Tukey's honest significant difference (HSD) tests *post hoc*-test using an alpha risk set at 5% was used to compare the parameters of interest (SPSS Inc. Version 29.0, Chicago, IL, USA).

FS data has been additionally described by a Weibull analysis. A common empirical expression for the cumulative probability of failure P at applied stress σ is the Weibull model (Weihull, 1951):

$$P_f(\sigma_c) = 1 - \exp\left[-\left(\frac{\sigma_c}{\sigma_0}\right)^m\right] \quad \text{(Equation 2)}$$

where σ_c is the measured strength, m the Weibull modulus and σ_0 the characteristic strength, defined as the uniform stress at which the probability of failure is 0.63. The double logarithm of this expression gives: $\ln\ln\frac{1}{1-P} = m\ln\sigma_c - m\ln\sigma_0$. By plotting ln ln(1/(1-P)) versus ln σ_c, a straight line results, with the upward gradient m, whereas the intersection with the x-axes gives the logarithm of the characteristic strength (Weihull, 1951).

3. Results

The outcome of the 3-point bending tests are summarized in Table 2 and Fig. 1. A multifactorial analysis showed a significant ($p < 0.001$) but small influence of surface finishing on the measured properties in descending order of the effect strength on E ($p < 0.001$; $\eta_p^2 = 0.326$) and FS ($\eta_p^2 = 0.105$), while this was not significant on the mirror constant A ($p = 0.505$) and on ε% ($p = 0.106$). In comparison, the effect of material on the measured parameters was higher and decreased from E ($\eta_p^2 = 0.528$) towards FS ($\eta_p^2 = 0.325$), ε% ($\eta_p^2 = 0.091$) and then A ($\eta_p^2 = 0.087$).

Within each surface treatment, one-way ANOVA evidenced three homogeneous subgroups for E data, in the following material sequence: AF5 > V > BFP ($p < 0.001$). The flexural strength FS was less discriminative across surface treatments, with statistically similar values for V and AF5 ($p = 0.81$ for P1200 treatment; 0.989 for polished and 0.42 for untreated specimens), both of which were significantly higher as BFP ($p < 0.001$). Since surface treatment has no influence on A, the data were merged and showed significantly similar values for V and BFP ($p = 0.228$) both higher compared to AF5 ($p < 0.001$).

Table 2
Variation of measured parameters (flexural strength (FS), Weibull modulus (m), mirror constant (A), flexural modulus (E), beam deflection (ε), arithmetic average of profile height deviations from the mean line (Ra) and peak to valley height (Rz)) with material and surface treatment. Within one material, values denoted by the same superscript are statistically similar. Tukey's HSD (honestly significant difference) post-hoc test (α = 0.05); SE = standard error; SD = standard deviation.

RBC	Surface finishing	FS [MPa] Mean +SD		m + SE		A [MPa$\sqrt{m}$] Mean +SD		E [GPa] Mean +SD		ε% Mean (SD)	Ra [μm] Mean (SD)	Rz [μm] Mean (SD)
AF5	P1200	152.8^{a}	15.4	11.9^{a}	0.38	1.93^{a}	0.20	6.7^{a}	0.6	2.5^{b} (0.2)	0.230 (0.04)	1.433 (0.27)
	polished	136.4^{b}	18.0	9.0 ^{b}	0.31	1.89^{a}	0.33	6.6^{a}	0.7	2.2^{a} (0.4)	0.034 (0.01)	0.413 (0.08)
	untreated	130.3^{b}	14.5	10.2^{b}	0.45	1.85^{a}	0.24	6.0^{b}	0.6	2.3^{ab} (0.3)	0.030 (0.01)	0.307 (0.06)
V	P1200	143.3^{a}	21.2	7.7^{a}	0.22	1.90^{a}	0.27	6.0^{a}	0.6	2.7^{a} (0.6)	0.281 (0.05)	1.673 (0.32)
	polished	137.1^{a}	23.4	6.8^{a}	0.22	2.07^{b}	0.35	6.2^{a}	0.6	2.5^{a} (0.6)	0.019 (0.00)	0.180 (0.03)
	untreated	135.7^{a}	13.7	11.9^{b}	0.77	2.16^{b}	0.25	5.6^{b}	0.5	2.7^{a} (0.4)	0.035 (0.00)	0.281 (0.05)
BFP	P1200	120.9^{a}	12.8	10.8^{a}	0.39	2.17^{a}	0.26	5.6^{a}	0.5	2.3^{a} (0.3)	0.155 (0.03)	1.148 (0.22)
	polished	114.0^{ab}	11.5	12.0^{a}	0.34	2.00^{b}	0.25	5.3^{a}	0.6	2.3^{a} (0.3)	0.028 (0.01)	0.302 (0.06)
	untreated	112.7^{b}	10.5	12.8^{a}	0.43	1.89^{b}	0.26	4.1^{b}	0.6	2.8^{b} (0.3)	0.052 (0.01)	0.317 (0.06)

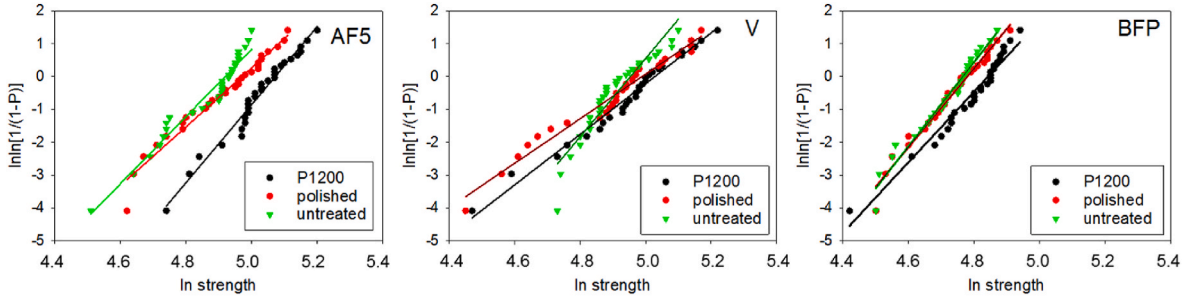

Fig. 1. Weibull plot representing the empirical cumulative distribution function of strength data. Linear regression was used to numerically assess goodness of fit and estimate the parameters of the Weibull distribution, as summarized in Table 2.

The material reliability (Fig. 1) expressed by the Weibull parameter, m, was comparable in all materials. Within the 95% confidence interval, the limits of which were calculated by subtracting and adding 1.96 times the standard error to the mean (Table 2), material reliability in BFP was not affected by surface treatment and was slightly higher for the P1200 treatment in AF5 and for untreated surfaces in V.

The structural appearance of the filler system is shown in Fig. 2 and was determined by Fe-SEM analysis operated in electron backscatter diffraction mode. This enable to differentiate the appearance of the filler depending on its chemical composition, as elements with a higher atomic order appear brighter. Larger, bright, compact and irregular fillers are observed in BFP along with round fillers that appear darker gray (contain elements of lower atomic order) and pre-polymerized fillers (PPFs) with irregular geometry. No PPFs were identified in V and AF5, only compact fillers with irregular shape, large filler size distribution and similar composition, while the maximum filler size in V

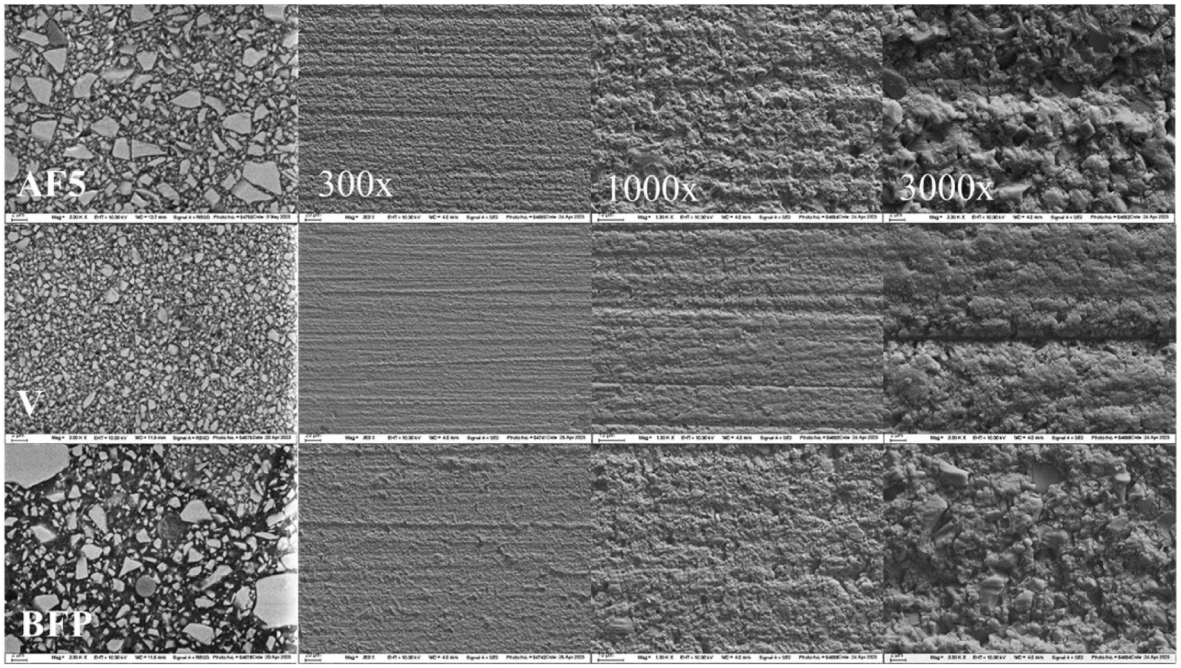

Fig. 2. Fe-SEM evaluation of the filler at 3000× magnification on polished specimens (left) followed by evaluation of sample surface after P1200 treatment at progressively higher magnification (300×, 1000x, 3000x) for the analyzed materials.

appears significantly smaller compared to AF5.

For the P1200 treatment, Fe-SEM evaluation at progressively higher magnification (300×, 1000x, 3000x) shows a smoother surface appearance in V, while larger fillers in AF5 and BFP were either exposed or pulled-out from the organic matrix during grinding (3000 magnification).

In addition to the structural appearance of the filler system, 3D surface images are displayed in Fig. 3a–c for each material and surface treatment. The peak to valley height for P1200 surface processing are varying from +0.671 μm to −1.088 μm, which corresponds to a range of 1.759 μm. The prevalence of deeper areas (blue marking in the corresponding scale in Fig. 3a) is higher in AF5 and V, while these areas appear rarer and smaller in BFP.

In polished specimens, the difference between peaks and valleys is 4.5x lower and amounted 0.403 μm (0.122 and −0.281, Fig. 3b). The smoothest surface is evident in V. Large, medium-deep areas (−0.16 μm) are observed in BFP, which can be assigned to the PPFs based on their shape and size. In comparison, AF5 has a higher number of smaller, deeper (−0.281 μm) and homogeneously distributed pits. Interestingly, the roughness range is larger for the untreated samples than for the polished ones and the peak to valley height amounted 0.766 μm (0.191 and −0.575, Fig. 3c), while no clear difference between the materials is evident. This qualitative description of the 3D images is reflected quantitatively by the 2D parameters R_a and R_z summarized in Table 2, which confirm that roughness results for polished specimens are slightly lower compared to no treatment (except for AF5), both lower compared to the P1200 treatment. The smaller filler size in V is clearly reflected in a smoother polished surface, while the surface in the P1200 treatment in BFP was less rough compared to AF5 and V.

Surface finishing influenced less the fracture mode. Failures initiated by volume defects were the most common failure mode (77.4%) with surface defects accounting for 14.4% (edge) and 7.0% (corner) and 1.1% (3 out of 270) were not evaluable (n. e.). A polished surface does not necessarily result in a lower prevalence of surface located defects. A detailed fracture mode distribution is shown in Fig. 4 for each material and surface treatment.

Examples of the observed fracture modes across the materials and surface treatments are presented in Fig. 5. Arrows mark the edge of the fracture mirror (smooth surface in the initial part of the fracture created when the crack is accelerated) and point to the origin of the fracture, which is enlarged in the image below and is located in the tensile zone of the sample. The rougher surface adjacent to the mirror (mist) is followed by crack propagation in different directions, resulting in radial striations (hackle lines).

4. Discussion

Surface treatment plays an important role in determining the interaction of a composite sample or filling with its environment (Lohbauer et al., 2008), as rough surfaces can form sites able to initiate cracks, wear faster, and have higher coefficients of friction than smooth surfaces (Ren et al., 2021). All of these aspects are relevant both in vitro and in vivo.

In a clinical situation, a composite filling is polished after being placed in the patient's mouth. Some areas may be clinically difficult to reach for polishing, so the oxygen inhibition layer formed on the surface cannot be removed. These two scenarios, along with surface roughening that may occur during clinical wear or tooth brushing, were simulated in the present study. The surface treatments listed are also relevant for in vitro material testing, especially since the handling of the surface of a composite sample is not clearly specified in the standards used for material evaluation.

To account for the dependence of surface treatment on the materials' intrinsic roughness induced by microstructural particularities and filler sizes, three very different materials were selected for the experiment. The Ormocer-based composite AF5 (organically modified ceramics (Schmidt and Wolter, 1990)), uses a polymer matrix that was originally developed for coatings (Schmidt and Wolter, 1990) and is characterized by high abrasion resistance (Tagtekin et al., 2004a, 2004b). It consists of pre-crosslinked inorganic networks based on polysiloxanes that are produced using the sol-gel process (Schmidt, 1992). The inorganic Si–O–Si network, produced by hydrolysis and polycondensation reactions, is cross-linked by multifunctional urethane and thioether (meth)acrylate alkoxysilanes in the polymerization reaction (Schmidt, 1990). The inorganic fillers used are rather large, irregular and have dimensions of up to 6 μm, as illustrated in Fig. 2. The material has the highest inorganic filler content in the range of selected materials, which was clearly reflected in the highest flexural modulus. Venus (V) is a universal hybrid composite that is recommended for use in both the anterior and posterior tooth areas. It contains compact, irregularly shaped inorganic fillers, which are significantly smaller compared to the other two materials and have a maximum size of ca. 2 μm and a homogeneous filler distribution (Fig. 2). With a similar matrix composition as V (Table 1) but the lowest filler amount BFP is classified as a flowable composite. In addition to compact glass fillers, it also contains large pre-polymerized as well as pre-reacted glass ionomer fillers (PRG) (Roberts et al.). PRG fillers consist of fluoroaluminosilicate glass that has reacted with a polyalkenoic acid in the presence of water to form a wet siliceous hydrogel, which is subsequently freeze-dried, desiccated, milled and silanized (Roberts et al.; Ikemura et al., 2008).

One of the important observations of the present study that needs to be highlighted is the independence of the ranking of materials in terms of E and FS from surface treatment. Observed differences in the measured properties are therefore directly attributed to the composition and microstructure of the materials. The flexural modulus undoubtedly ranks the materials according to the content of inorganic fillers. Strength is less discriminatory as it must take into account additional influencing factors, including the location and type of critical flaws able to initiate fracture. As material testing occurred under bending, a gradient of tensile to compressive stress is generated (Mecholsky, 1995) with the crack-initiating flaw located on the tensile side of the specimens and the crack propagating in the direction of the neutral axis. The fact that the ranking of the materials in terms of flexural strength is independent of surface treatment is confirmed by qualitative fractography, as surface treatment did not fundamentally altered the fracture pattern and the dominant fracture mechanism in all groups was initiated by volume defects. During surface treatment, it occasionally occurred that these volume defects were opened when close to the surface, as illustrated by the incomplete spherical shape of the defect in Fig. 5A. In such a case, the defect that initiated the fracture was classified as located on the surface. Its size of ca. 20 μm is significantly larger than the flaws induced by roughening. The fact that open porosities are often the cause of fracture is consistent with the observation that polished surfaces do not reduce the amount of surface defects in any of the materials tested. Similarly, both surface-treated sample groups in Venus, either polished or roughened, were found to have lower reliability than the samples that retained the oxygen inhibition layer, which seems surprising at first glance. This aspect was in fact specific to V, where larger voids distributed throughout the fractured surfaces were observed more frequently than in the other materials, providing a higher probability that these were opened during grinding and thus served as additional surface defects. This behaviour confirms a previous study for Venus that used the same sample preparation and geometry but a smaller sample size (n = 20) (Ilie, 2021). For the other two materials, the reliability was not affected by surface treatment (BFP) or it was at the limit of significance (AF5).

Since all four large sides of each parallelepiped specimens were processed, the specimen preparation was time consuming. It was done under controlled, automated conditions, which was well quantified in the final test specimen geometry. The geometry of the test specimen is predefined by the used mold, whereby the final dimensions for all specimens in terms of height and depth must meet the tolerance values specified in the ISO standard used (2.00 mm ± 0.10 mm). In this

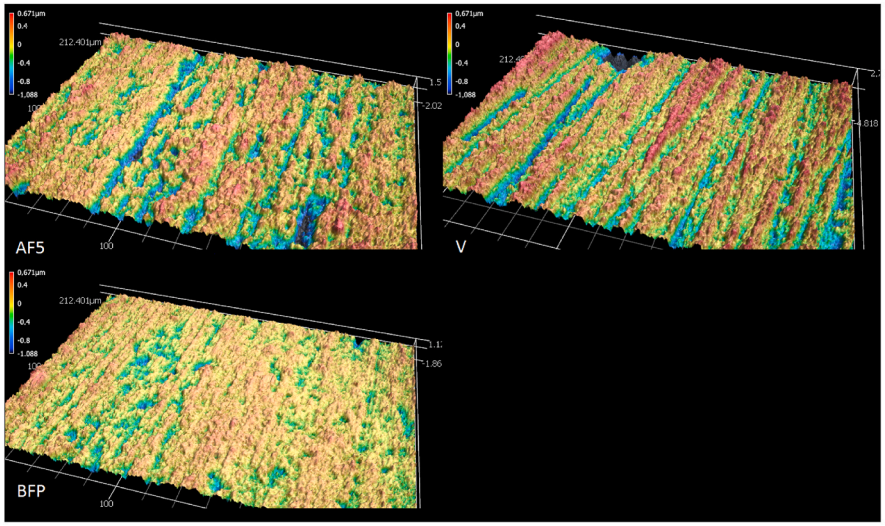

a) P1200

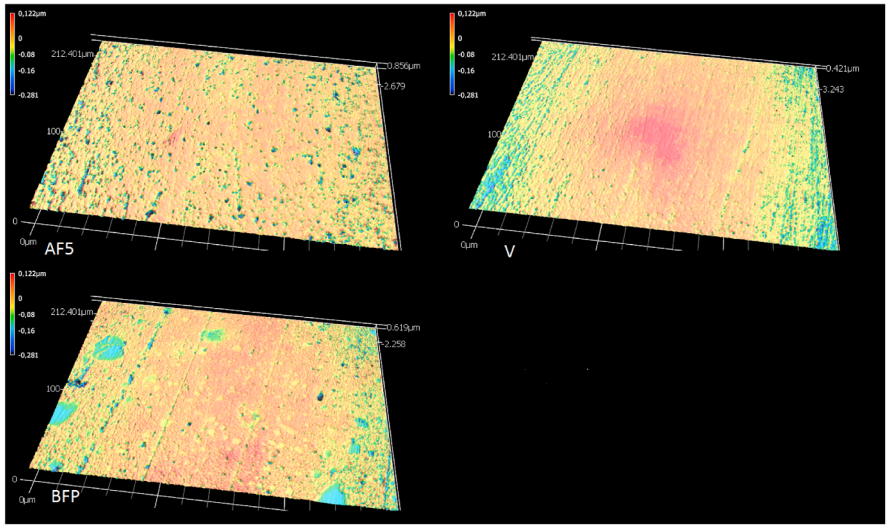

b) Polished

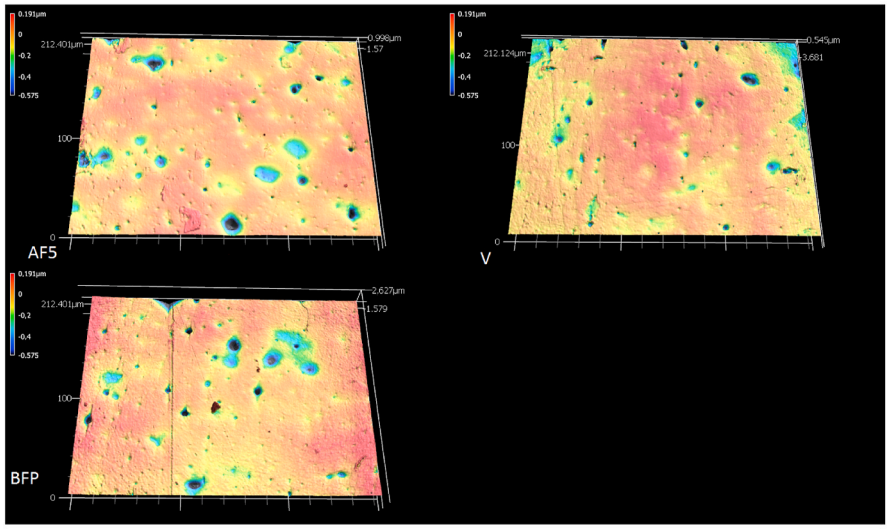

c) untreated

Fig. 3. 3D surface images depending on the treatment: a) roughening with SiC paper P1200, b) polishing up to P4000, and c) no treatment to maintain the oxygen inhibition layer.

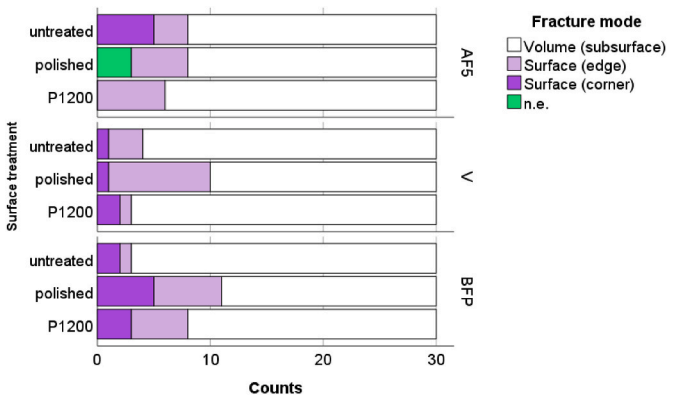

Fig. 4. Fracture mode distribution (n.e. = not evaluable) among analyzed materials and surface treatments.

context, the height varied less but significantly within the three different surface treatment in the sequence: untreated (2.14 ± 0.05 mm) > P1200 (2.10 ± 0.05 mm), p = 0.0531 > polished (2.01 ± 0.05 mm), p = 0.0531. Regarding depth, the dimensional changes were: untreated (2.05 ± 0.02 mm) > P1200 (2.07 ± 0.04 mm) and polished (2.07 ± 0.05 mm). The final dimensions confirm that the P1200 treatment only roughened the surface, without consistent material removal, and that on average no more than 130 μm was removed during roughening and polishing. The latter also confirms that the oxygen inhibition layer has been thoroughly removed, as in composites containing more than 50 wt % filler, the transition from oxygen inhibited to bulk polymer regions was located at depths of 5–10 μm, while increased viscosity was shown to limit oxygen diffusion and increase conversion near the surface, without necessarily modifying the depth of inhibition (Gauthier et al., 2005).

In addition to the location of the flaw that initiated the fracture, the fracture mirror radius measured along the tensile surface (Mecholsky et al., 1976) was used to determine the mirror constant A (Quinn et al., 2007; Ghelbere and Ilie, 2023). Since the mirror constant was independent of the surface treatment for all analyzed materials, the hypothesis that a material parameter was determined is strengthened. The connection with fracture toughness (Mecholsky et al., 1976) cannot be directly proven here, since K_{Ic} data is missing for some of the tested materials, but the physical interpretation of the parameter can definitely be related to resistance to crack propagation based on the microstructure of the materials. Apart from their influence on strength and the elastic modulus, filler amount, distribution, size and implicitly the distance between the fillers represent important parameters for optimizing toughness, since the presence of fillers in a polymer matrix hinders or requires more energy for the formation, growth and propagation of cracks (Khaund et al., 1977). Interestingly, the mirror constant was slightly lower in AF5, the material with the highest filler loading. It should not be ignored that the filler size was very large in AF5, offering a lower total filler matrix interface for crack energy dissipation through debonding of the fillers from the organic matrix compared to V. On the other side, the pre-polymer fillers in BFP help increasing fracture toughness as the crack growth may be retarded due to pre-polymer filler debonding, as the bond between pre-polymer fillers and the organic matrix is seen as weaker than the bond between the inorganic filler and the matrix.

5. Conclusions

It can be concluded that surface finishing has a small influence on FS and E within the considered roughness ranges, while the ranking of materials with regard to these parameters within a surface treatment is similar. This nevertheless justifies the need for standardization of surface processing for material testing. Due to the complexity of polishing the surface, treatment with 600 grit SiC paper is recommended. The mirror constant turned out to be independent of the surface treatment. The clear dominance of volume defects in all examined materials as a cause of fracture reduces the influence of roughness on the measured properties, as surface defects generated did not reach the critical flaw size. This insight was only possible through qualitative and quantitative research fractography.

CRediT authorship contribution statement

Nicoleta Ilie: Writing – review & editing, Writing – original draft, Visualization, Validation, Supervision, Software, Resources, Project administration, Methodology, Investigation, Funding acquisition, Formal analysis, Data curation, Conceptualization.

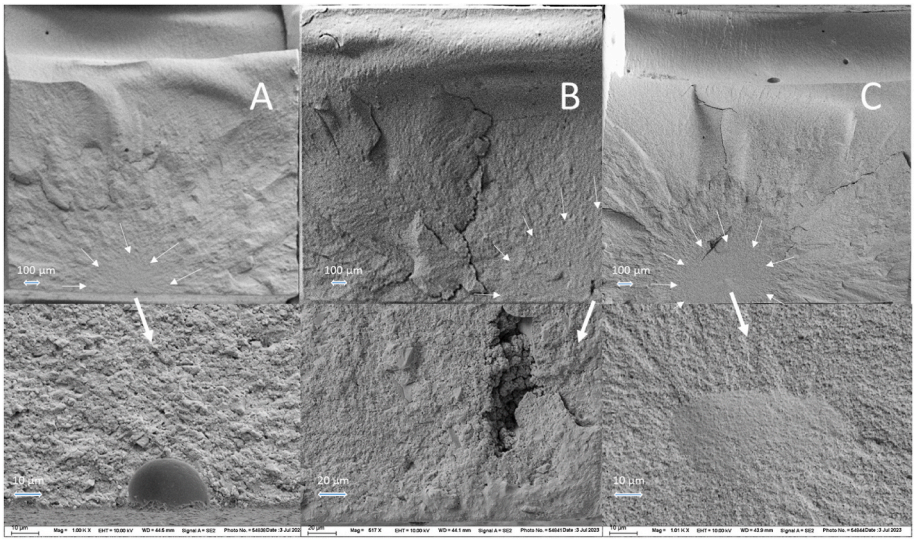

Fig. 5. Example of fractured specimens imaged by Fe-SEM: A = fracture originated from a surface defect, a porosity located on the edge (AF5, P1200; FS = 156.5 MPa; E = 5.9 GPa); B = fracture originated from a surface defect located at the corner (BFP, polished; FS = 125.76 MPa; E = 5.2 GPa); C = fracture originated from a volume (sub-surface) defect (V, P1200; FS = 146.1 MPa, E = 5.7 GPa).

Declaration of competing interest

The authors declare that they have no known competing financial interests or personal relationships that could have appeared to influence the work reported in this paper.

Data availability

Data will be made available on request.

References

Aboushelib, M.N., Elraggal, A., 2023. Fractographic analysis of fractured fixation screws in implant-supported restorations. Dent. Mater. 39, 123–131.

Amaya-Pajares, S.P., Koi, K., Watanabe, H., da Costa, J.B., Ferracane, J.L., 2022. Development and maintenance of surface gloss of dental composites after polishing and brushing: review of the literature. J. Esthetic Restor. Dent. 34, 15–41.

Bansal, G.K., Duckworth, W.H., 1977. Fracture stress as related to flaw and fracture mirror sizes. J. Am. Ceram. Soc. 60, 304–310.

Bollen, C.M., Lambrechts, P., Quirynen, M., 1997. Comparison of surface roughness of oral hard materials to the threshold surface roughness for bacterial plaque retention: a review of the literature. Dent. Mater. 13, 258–269.

Ferracane, J.L., 2011. Resin composite–state of the art. Dent. Mater. 27, 29–38.

Gauthier, M.A., Stangel, I., Ellis, T.H., Zhu, X.X., 2005. Oxygen inhibition in dental resins. J. Dent. Res. 84, 725–729.

Ghelbere, R., Ilie, N., 2023. Validation of the Orr theory in dental resin-based composites: a fractographic approach. J. Mech. Behav. Biomed. Mater. 144, 105982.

Griffith, A.A., Taylor, G.I., 1921. VI. The phenomena of rupture and flow in solids. Philos. Trans. R. Soc. Lond. - Ser. A Contain. Pap. a Math. or Phys. Character 221, 163–198.

Ikemura, K., Tay, F.R., Endo, T., Pashley, D.H., 2008. A review of chemical-approach and ultramorphological studies on the development of fluoride-releasing dental adhesives comprising new pre-reacted glass ionomer (PRG) fillers. Dent. Mater. J. 27, 315–339.

Ilie, N., 2021. Microstructural dependence of mechanical properties and their relationship in modern resin-based composite materials. J. Dent. 114, 103829.

ISO 4049:2019 Dentistry — Polymer-Based Restorative Materials: International Organization for Standardization. p. 29.

Johnson, J., Holloway, D., 1966. On the shape and size of the fracture zones on glass fracture surfaces. Phil. Mag.: A Journal of Theoretical Experimental and Applied Physics 14, 731–743.

Khaund, A.K., Krstic, V.D., Nicholson, P.S., 1977. Influence of elastic and thermal mismatch on the local crack-driving force in brittle composites. J. Mater. Sci. 12, 2269–2273.

Kirchner, H.P., Conway, Jr J., 1987. Criteria for crack branching in cylindrical rods: II, flexure. J. Am. Ceram. Soc. 70, 419–425.

Lohbauer, U., Müller, F.A., Petschelt, A., 2008. Influence of surface roughness on mechanical strength of resin composite versus glass ceramic materials. Dent. Mater. 24, 250–256.

Lohbauer, U., Amberger, G., Quinn, G.D., Scherrer, S.S., 2010. Fractographic analysis of a dental zirconia framework: a case study on design issues. J. Mech. Behav. Biomed. Mater. 3, 623–629.

Mecholsky, Jr JJ., 1995. Fractography: determining the sites of fracture initiation. Dent. Mater. 11, 113–116.

Mecholsky, J., Rice, R., Freiman, S., 1974. Prediction of fracture energy and flaw size in glasses from measurements of mirror size. J. Am. Ceram. Soc. 57, 440–443.

Mecholsky, J.J., Freimam, S.W., Rice, R.W., 1976. Fracture surface analysis of ceramics. J. Mater. Sci. 11, 1310–1319.

Øilo, M., Arola, D., 2018. Fractographic analyses of failed one-piece zirconia implant restorations. Dent. Mater. 34, 922–931.

Orr, L., 1972. Practical analysis of fractures in glass windows. Mater. Res. Stand. 12, 21.

Quinn, G.D., 1992. Room-temperature flexure fixture for advanced ceramics. NISTIR 4877. National Institute of Standards and Technology.

Quinn, G., 2007. Guidelines for measuring fracture mirrors. Ceram. Trans. 199, 163–190.

Quinn, J.B., Quinn, G.D., 2010. Material properties and fractography of an indirect dental resin composite. Dent. Mater. 26, 589–599.

Quinn, J.B., Quinn, G.D., Kelly, J.R., Scherrer, S.S., 2005. Fractographic analyses of three ceramic whole crown restoration failures. Dent. Mater. 21, 920–929.

Quinn, J.B., Scherrer, S.S., Quinn, G.D., 2007. The increasing role of fractography in the dental community. Ceram. Trans. 199, 253.

Ren, Y., Zhang, L., Xie, G., Li, Z., Chen, H., Gong, H., et al., 2021. A review on tribology of polymer composite coatings. Friction 9, 429–470.

Roberts T, Miyai K, Ikemura K, Fuchigami K and Kitamura T, inventorsFluoride ion sustained release preformed glass ionomer filler and dental compositions containing the same. United States Patent No. 5,883,1531999,.

Scherrer, S.S., Quinn, J.B., Quinn, G.D., Kelly, J.R., 2006. Failure analysis of ceramic clinical cases using qualitative fractography. Int. J. Prosthodont. (IJP) 19, 185–192.

Scherrer, S.S., Lohbauer, U., Della Bona, A., Vichi, A., Tholey, M.J., Kelly, J.R., et al., 2017. ADM guidance-Ceramics: guidance to the use of fractography in failure analysis of brittle materials. Dent. Mater. 33, 599–620.

Schmidt, H.K., 1990. Aspects of Chemistry and Chemical Processing of Organically Modified Ceramics, 180. MRS Online Proceedings Library (OPL), p. 961.

Schmidt, H.K., 1992. Sol-Gel Synthesis of Ceramic-Organic Nano Composites, 274. MRS Online Proceedings Library (OPL), p. 121.

Schmidt, H., Wolter, H., 1990. Organically modified ceramics and their applications. J. Non-Cryst. Solids 121, 428–435.

Tagtekin, D.A., Yanikoglu, F.C., Bozkurt, F.O., Kologlu, B., Sur, H., 2004a. Selected characteristics of an Ormocer and a conventional hybrid resin composite. Dent. Mater. 20, 487–497.

Tagtekin, D., Tan, C., Chung, S., 2004b. Wear behavior of new composite restoratives. Operat. Dent. 29, 269–274.

Weihull, W., 1951. A statistical distribution function of wide applicability. J. Appl. Mech. 18, 290–293.

Yoffe, E.H., 1951. The moving griffith crack. London, Edinburgh Dublin Phil. Mag. J. Sci. 42, 739–750.